

INVERSE PROBLEMS RELATED TO ION CHANNEL SELECTIVITY*

MARTIN BURGER[†], ROBERT S. EISENBERG[‡], AND HEINZ W. ENGL[§]

Abstract. Ion channels control many biological processes in cells, and, consequently, a large amount of research is devoted to this topic. Great progress in the understanding of channel function has been made recently using advanced mathematical modeling and simulation. This paper investigates another interesting mathematical topic, namely inverse problems, in connection with ion channels. We concentrate on problems that arise when we try to determine (“identify”) one of the structural features of a channel—its permanent charge—from measurements of its function, namely current-voltage curves in many solutions. We also try to design channels with desirable properties—for example with particular selectivity properties—using the methods of inverse problems. The use of mathematical methods of identification will help in the design of efficient experiments to determine the properties of ion channels. Closely related mathematical methods will allow the rational design of ion channels useful in many applications, technological and medical. We also discuss certain mathematical issues arising in these inverse problems, such as their ill-posedness and the choice of regularization techniques, as well as challenges in their numerical solution. The L-type Ca channel is studied with the methods of inverse problems to see how mathematics can aid in the analysis of existing ion channels and the design of new ones.

Key words. ion channels, Poisson–Nernst–Planck equations, identification, optimal design, permanent charge, current-voltage relations

AMS subject classifications. 35R30, 92C05, 92C40, 65N21, 65R32

DOI. 10.1137/060664689

1. Introduction. Ion channels are proteins with a hole down their middle that allow ions to move through otherwise impermeable cell membranes, thereby controlling many biological processes of great importance in health and disease. Interest in channels has grown rapidly because of their general role as controllers of biological function in health and disease. A quick glance at the literature through a search on the Internet will find hundreds of papers on channelopathies, diseases of channels (cf. [As99, LHJR00]). Specifically, channels are proteins akin to enzymes (cf. [Ei90]) that control the flow of ions through membranes and thus control a wide range of biological functions (cf. [Aletal94, Hi01]).

Channels generate the action potential which conducts all information in the nervous system and coordinates contraction, including the contraction which allows the heart to function as a pump. Channels are involved in nearly all sensory function, in the secretion of hormones, and in the function of the kidney and intestine. There is hardly a biological function that is not controlled by channels or transporters in an important way.

*Received by the editors July 10, 2006; accepted for publication (in revised form) January 22, 2007; published electronically April 24, 2007.

<http://www.siam.org/journals/siap/67-4/66468.html>

[†]Institut für Industriemathematik, Johannes Kepler Universität, Altenbergerstr. 69, A-4040 Linz, Austria. Current address: Institut für Numerische und Angewandte Mathematik, Westfälische Wilhelms-Universität Münster, Einsteinstr. 62, D-48149 Münster, Germany (martin.burger@uni-muenster.de).

[‡]Department of Molecular Biophysics and Physiology, Rush University Medical Center, 1750 W. Harrison St., Chicago, IL 60612 (beisenbe@rush.edu). This author’s work was supported in part by NIH grant GM076013.

[§]Institut für Industriemathematik, Johannes Kepler Universität, Altenbergerstr. 69, A-4040 Linz, Austria (heinz.engl@jku.at).

The enormous importance of channels has generated enormous amounts of experimental work. Literally hundreds of laboratories and thousands of scientists measure channel properties every day with remarkable resolution, often studying the properties of just one protein molecule. Molecular genetics and molecular biology allow routine (although tedious) engineering of channel proteins nearly one atom at a time (cf. [Mietal06]). Few areas of biology are so well explored at such resolution.

Channels also are much simpler than enzymes. Channel function does not involve changes in covalent bonds or chemistry in that sense. Channels perform many of their functions without changing structure (on the biological time scale of msec). Ions move through channels driven by concentration gradients and electrical potential at room temperature. Channels form an unusual nearly unique system because they are both physically simple and biologically very important. The daunting complexity of the structure of many biological systems is not found in single molecules of channel proteins [TBSS01, Ei98, Maetal03].

One of the defining characteristics of proteins is their selectivity. Most proteins bind specific organic chemicals with great specificity even at very low concentrations, 10^{-5} times smaller than concentrations of ions always associated with proteins, e.g., K^+ , Na^+ , and Cl^- , which are typically found at 0.2 M concentration. These organic molecules often control the biological function of the protein with great specificity even at these very low concentrations. Ion channels (for example) conduct ions of one type much better than ions of another type, and this selectivity among ions is essential for their role in signaling in the nervous system, and coordination of muscle contraction, particularly in the heart. If the selectivity of ion channels is understood, and a physical theory is available showing how channel structure produces channel function, channel proteins can be designed to specification and built using the well-developed techniques of molecular engineering, e.g., by site-directed mutagenesis.

The design of ion channels to specification can also be seen as an application of the mathematical theory of inverse problems (“reverse engineering”). Design requires specialized mathematics because of the complexity and sensitivity (with respect to perturbations) of the system and the mutual dependence of various design goals: improving some properties can make others worse, and so mathematics is needed to find a good compromise. In this paper, we show how iterative and variational regularization methods developed for inverse problems can be applied to design or identify the function—in particular the selectivity—of ion channels using the physical chemistry of crowded charge, which is modeled through the Poisson–Nernst–Planck equations, a system of nonlinear partial differential equations combined with a density functional theory of excess chemical potential. The main idea of this approach is to formulate the design or identification of permanent charge as an abstract operator equation or optimization problem involving Poisson–Nernst–Planck (or related) models for the flow of electrical charge through the channel and to regularize it either by using an iterative method with appropriate stopping criterion and/or additional penalization of the objective functional. This regularization is necessary to compute numerical solutions in a stable and robust way, since the inverse problem is ill-posed in the sense that small differences in the electrical current can correspond to arbitrarily large differences in the permanent charge. In the context of identification, regularization methods allow computation of a stable approximation to the permanent charge in the channel. In the context of design, they also allow us to introduce a priori ideas of suitable designs.

Inverse problems arise whenever one searches for causes of desired or observed effects. Two problems are called inverse to each other if the formulation of one problem involves the solution of the other one. At first sight, it might seem arbitrary which of

these problems is called direct and which is called inverse. Usually, the direct problem is the more classical one. But there is an intrinsic mathematical reason to call one problem “inverse,” namely the fact that it is usually ill-posed (cf. [EHN96]). When dealing with partial differential equations, the direct problem usually predicts the evolution of the described system from knowledge of its present state and the governing physical laws including information on all physically relevant parameters. A possible inverse problem would be to compute (some of) the parameters from observations of the evolution of the system; this particular inverse problem is called “parameter identification” and is usually ill-posed (cf. [CER90, EHN96, ER95, IS05, Na06]). We shall highlight the ill-posedness of the inverse problem in a simplified setup, which we nonetheless expect to capture the essential features of the problem, and we also discuss *identifiability*, i.e., the question of whether the unknowns in the inverse problem are determined uniquely from the data.

Regularization methods are needed to overcome these instabilities and to design solution techniques that are robust (i.e., that are stable with respect to data and numerical errors). In general terms, regularization methods replace an ill-posed problem by a family of neighboring well-posed problems. We perform this task for design and identification problems in ion channels. In addition to the stable approximation, the regularization methods are also used to introduce a priori knowledge about the ion channel structure. In a case study of an L-type Ca channel, we present various numerical results, which demonstrate the feasibility of our approach and highlight some particular issues that are likely to appear in channel and protein problems.

2. Modeling ion channels. In the following, we give a brief overview of continuum models of ion transport through channels. Such models need to incorporate the electrostatic interaction between the charged particles, the change of charge density by the mobile ions and a consequent change of the electric field, the generation of ion flux by the electric field, and the direct electrochemical interactions between the ions. Here we shall detail and use Poisson–Nernst–Planck (PNP) models, where the unknowns are the electric potential V and the densities ρ_k of the various (ionic) species present in the channel. Continuum models of this sort have received much attention in the literature (cf. [CE93, GNE02, GNE03, IR02a, IR02b, Maetal03, NCE00]) as well as criticism, mostly because they neglect correlations produced by the small number of ions that can fit into a single channel. Correlations can be included in the derivation of PNP (cf. [SNE01, NHE03]), and certain types of correlations can be analyzed and included in generalizations of PNP with some success (cf. [GNE02, GNE03, Maetal03, SNE01, XWGM06]). Much more work is needed in this regard, and it remains to be seen how well extensions of PNP can deal with the entire set of correlations present in particle-based simulations. Despite similar limitations, continuum models are used very widely in many fields: For example, in computational electronics, continuum models are widely used because they are typically much faster than particle-based simulations (cf. [Se84, JaLu89]).

In our work, we use the extended form of PNP as found in [GNE02, GNE03], understanding that we will need to refine and replace this model as it is improved. The following sections show how our inversion approach can easily be updated to possibly improved forward models.

We assume that the total number of different species is M , but we distinguish between the free species and the species confined to the channel, which create the permanent charge of the channel. For simplicity, we restrict ourselves to a single confined species, denoted with index M , but extensions to multiple confined species

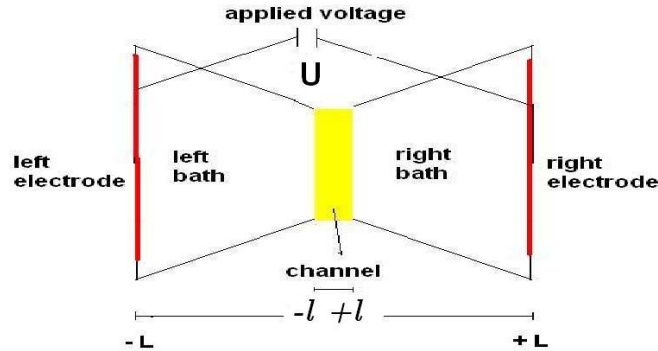


FIG. 1. Two-dimensional sketch of the computational domain Ω modelling the bath-channel system.

are possible. We mention that selectivity in an ion channel can occur only if $M \geq 4$, since one needs at least two free species with charges of the same sign in order to have selectivity of one over the other, as well as a confined species (permanent charge) and a free species of opposite sign to achieve charge neutrality in the bath. Since the bath and channel in practice always includes water, the number of densities should satisfy $M \geq 5$. Indeed, in the case of an L-type Ca channel we study in further detail below, the number of species is exactly equal to five.

The concentrations have to be computed in a domain Ω that describes the bath and channel. A schematic setup of Ω is depicted in Figure 1.

The electric potential is computed from the Poisson equation with a source term equal to the charge generated by the ions, including the permanent charge. For the continuum description of ion transport, the Nernst–Planck (NP) equations are used, which involve a diffusion term as well as a drift term caused by the electric field (ideal electrostatic potential), an external confining potential, and the excess electrochemical potential. A computational model is a coupled system of the form (after suitable scaling)

$$(2.1) \quad -\lambda^2 \Delta V = \sum_k z_k \rho_k,$$

$$(2.2) \quad -\nabla \cdot (m_j \rho_j \nabla \mu_j[\rho_1, \dots, \rho_M; V]) = 0, \quad j = 1, \dots, M.$$

Here z_k denotes a relative charge of the k th species, m_j is the mobility, and λ is a scaled variable depending on the dielectric coefficient, elementary charge, and typical values of the concentrations ρ_k . The potentials μ_k are computed as variations of an energy functional, i.e.,

$$(2.3) \quad \mu_k = \frac{\partial}{\partial \rho_k} E[\rho_1, \dots, \rho_M; V],$$

which is of the form

$$(2.4) \quad E[\rho_1, \dots, \rho_M; V] = \int_{\Omega} \left(-\lambda^2 |\nabla V|^2 + \sum_k (z_k V \rho_k + c_k \rho_k \log \rho_k + \mu_k^0 \rho_k) \right) dx \\ + E^{ex}[\rho_1, \dots, \rho_M].$$

The functional E includes electrostatic interaction via the electric field (the first two terms), diffusion (the logarithmic term), external forces via potentials μ_k^0 , and direct electric and chemical interactions. Note that the Poisson equation (2.1) can be seen as an equilibrium condition for this energy, i.e.,

$$(2.5) \quad 0 = \frac{\partial}{\partial V} E[\rho_1, \dots, \rho_M, V].$$

Besides the specific exchange terms in energy and potentials, the PNP equations (2.1), (2.2) are a standard model for electrodiffusion of charged species (cf. [Ru90]), which has well-known applications to semiconductors (cf. [VR50, MRS90]). A major difference between electrodiffusion of ions and semiconductors is that it is easy to control the concentrations of the different species in the bath independently of the applied potential, while it is not easy (or even usually possible) to control the concentration of holes or electrons independent of the contact potential. Boundary conditions for the ion channel problem are of the form

$$(2.6) \quad \begin{aligned} V &= U && \text{on } \Gamma_D, \\ \rho_j &= \eta_j && \text{on } \Gamma_D, \quad j = 1, \dots, M-1, \\ \frac{\partial \mu_M}{\partial n} &= 0 && \text{on } \Gamma_D, \\ \frac{\partial V}{\partial n} &= 0 && \text{on } \Gamma_N, \\ \frac{\partial \mu_j}{\partial n} &= 0 && \text{on } \Gamma_N, \quad j = 1, \dots, M. \end{aligned}$$

Here the boundary is split into $\partial\Omega = \Gamma_D \cup \Gamma_N$, where Γ_N is the insulated part and $\frac{\partial}{\partial n}$ denotes the normal derivative. Since there are usually two baths, Γ_D will consist of two separated components, and the boundary values are typically constant on each component. The potential U (or, rather, the difference of U between the left and right bath) denotes an applied voltage, and η_j are the bath concentrations of the free species, which are constrained by the charge neutrality condition

$$(2.7) \quad \sum_{j=1}^{M-1} z_j \eta_j = 0.$$

Note that the confined species is usually modeled at equilibrium, which is equivalent to the zero flux boundary condition (for the constrained ions) on the whole boundary. The total number of confined particles N_M needs to be specified to determine ρ_M , giving

$$(2.8) \quad \int_{\Omega} \rho_M dx = N_M.$$

The (measured) output of a channel is the current flowing out on one side, given by

$$(2.9) \quad I = \sum_{k=1}^{M-1} \int_{\Gamma_0} z_k J_k \cdot dn,$$

where $\Gamma_0 \subset \Gamma_D$ is one of the connected components of Γ_D and J_k denotes the flux of species k given by

$$(2.10) \quad J_k = -\rho_k \nabla \mu_k = -c_k \nabla \rho_k - z_k \rho_k \nabla V - \rho_k \nabla \mu_k^0 - \rho_k \nabla \mu_k^{ex},$$

where the excess potential is defined as $\mu_k^{ex} = \frac{\partial E^{ex}}{\partial \rho_k}$. The current can also be measured and computed from the charge induced on surrounding (Dirichlet) boundaries using the Shockley–Ramo theorem (cf. [NPG04]).

We mention that the nondimensionalization and scaling of (2.1), (2.2), (2.6) can be performed in an analogous way to the drift-diffusion model for semiconductors (cf. [MRS90]), and for typical values one also has to expect that λ is small; i.e., the Poisson equation (2.1) becomes a singularly perturbed problem.

The system just described has to be coupled to some model for the excess potentials. The excess electrochemical potentials (obtained as variations of the excess energy with respect to the particle densities) include the direct interactions between the ions, usually obtained from hard-sphere or Lennard-Jones models. The external confining potential describes the external forces produced by the structure of the channel on the ionic groups of the protein that make up the permanent charge. This confined permanent charge produces the selectivity of the channel. For our test computations detailed below, we use a specific model of the other components of the excess potential based on density-functional theory (DFT), as described in [GNE02, GNE03, NCE00]. Other models of the excess electrochemical potential require similar computational schemes and lead to the same kind of inverse problems. For a detailed statement of all equations used in the computation of the excess potentials we refer to the appendix of [BEE06].

3. Inverse problems in ion channels. As in many inverse problems, we consider two classes of inverse problems in ion channels, which have different practical motivations:

- *Identification problems* consist in determining properties of a “real” channel (permanent charge and structure), given measurements of the channel output (the total current, in a standard experimental setting) at various different conditions (applied voltages, bath concentrations of the ions).
- *Design problems* consist in determining properties of a “synthetic” channel—either a modification of a natural channel (cf. [Mietal06]) or an abiotic analogue of a biological channel (cf. [Sietal06])—such that optimal characteristics are obtained with respect to some criterion (e.g., selectivity with respect to certain ion species). The medical and technological effects of improved selectivity can be very important. For example, improving Ca selectivity in the L-type Ca channel (by using a drug that changes permanent charge in a way mathematics suggests, if such a drug can be made) would be medically relevant.

The unknowns to be identified or designed are related to the permanent charge, i.e., the ion species confined to the channel. First, an important number is the total

amount of permanent charge, i.e., the number N_M of charged particles confined to the channel. A second important quantity determining the permanent charge is the external confining potential μ_M^0 , which represents the forces acting on the permanent charge and encodes the channel structure. In the absence of an electrical field and of electrochemical interaction with other ions, the permanent charge density is given by

$$(3.1) \quad \rho_M = \gamma_M N_M \exp(-\mu_M^0/z_k)$$

with a constant γ_M determined from the condition (2.8). Hence, the number N_M and the confining potential μ_M^0 determine the permanent charge density and, subsequently, the selectivity properties of the channel. If the sensitivity of the permanent charge density ρ_M with respect to voltages and bath concentrations in the measured range appears to be negligible, one can also try to directly infer ρ_M from the measurements, ignoring the NP equation for ρ_M . The total charge N_M is a single positive number for which a lower bound (zero) and an upper bound (since too large permanent charges would destroy the channel) are available, and thus it could even be determined by sampling all its possible values. The ill-posedness plays no significant role in the determination of N_M . The confining potential μ_M^0 (and also the density ρ_M as an alternative) is a function of space, so that the inverse problem of determining the confining potential is infinite-dimensional. Since ill-posedness in the sense of discontinuous dependence on data arises only for infinite-dimensional problems and numerical instability becomes more severe as the number of unknowns/design parameters in the inverse problems increases (cf. [EHN96]), instability effects are expected to be more significant for determining the confining potential than for determining the total charge. As a consequence of the ill-posedness, suitable regularization methods have to be used to compute stable approximations of the confining potential, as explained in the previous sections. In the following, we will describe the computational solution of the inverse problems of determining total charge and confining potential in detail, both in the cases of identification and of design.

3.1. Identification. The aim of the identification problem is to find the total charge and/or the confining potential from measurements of the outflow current I taken at different bath concentrations η_j (boundary values of the densities ρ_j) and at different applied voltages U (boundary values of the electric potential V). The measured current I is one real number for each combination of voltage and bath concentrations. In general, I can be seen as a functional of voltage and bath concentrations. The underlying forward model creates a relation between the input P and the output I , which can be modeled via a nonlinear operator $F : P \mapsto I$ between function spaces. Note that the evaluation of the operator F for a specific value of P involves the solution of forward problems with given P for each combination of voltage and bath concentrations (in the idealized setting an infinite number of forward problems). In this setup, the identification problem can be formulated as the operator equation

$$(3.2) \quad F(P) = I^\delta,$$

where I^δ denotes the noisy version of the current obtained from measurements.

We mention that this identification problem has many similarities to the identification of *doping profiles* (i.e., permanent charges) in semiconductor devices from electrical measurements, a problem which has been investigated in detail previously (cf. [BEMP01, BEM02, BELM04, LMZ06, Wo06, WB06]). Since the underlying differential operators appearing in the forward model are exactly the same, one may

expect similar mapping properties of the forward operator F . In particular, this analogy suggests that the identification problem in ion channels (concerning the permanent charge density or the associated constraining potential) is severely ill-posed, as was found in some cases for semiconductors (cf. [BEMP01]). Below we shall also provide analytical arguments for a simplified model and numerical ones for the full model confirming the severe ill-posedness.

We also want to highlight some important differences between the identification problem for the permanent charge of ion channels and the already known identification of doping profiles in semiconductors. First, the forward models include additional effects such as the higher number of species, the excess electrochemical potentials, the different boundary conditions, and the model for the permanent charge density depending on the constraining potential. The second and most important difference is the amount of data that can be used. For semiconductors, only the voltage can be varied, but the boundary concentrations (of electrons and holes) are fixed. As a consequence, the amount of data is not enough to produce a unique solution of the inverse problem using current measurements (cf. [BEM02, Wo06]). On the other hand, one can also measure capacitances in the case of semiconductors (i.e., variations of the total charge with respect voltage change), which can significantly improve the quality of reconstructions in the case of unipolar devices (cf. [Wo06]), but measurements of nonlinear capacitance in biological systems are not analogous (cf. [BeSt98]). However, even with additional capacitance measurements, there are examples of nonuniqueness for the identification of doping profiles in bipolar devices due to an inherent antisymmetry caused by the special boundary values in semiconductors (cf. [Wo06]). Boundary values cover a wide range in an ion channel, and so this antisymmetry is broken, and uniqueness in the identification becomes more likely.

For semiconductors, it has already been shown that very demanding problems such as the inverse conductivity problem with a measured Dirichlet-to-Neumann map arise as special cases, and the full inverse dopant profiling is even more complex (cf. [BEMP01]). Since the measured currents and capacitances are functions of a single variable—the voltage—in semiconductors, the evaluation of the corresponding forward map F involves significantly fewer numerical solutions (“solves”) than in the case of ion channels, where the PNP system (2.1), (2.2) has to be solved for varying bath concentrations as well as voltage. Consequently, the computational complexity of the identification problem is even higher for ion channels and seems to be one of the most challenging inverse problems with respect to this issue. Because of the high number of solves of the PNP system, it is of fundamental importance to use efficient numerical schemes for the forward problem. Here we use a mixed finite element scheme with a novel symmetric linearization, which allows an efficient and robust solution of PNP systems with input parameters that cover a wide range of values (cf. [BW07]). The fact that currents are measured for many different setups in ion channel experiments is of crucial importance for the quality of reconstructions. Since the data set is richer than for semiconductors, one can actually achieve more ambitious goals in the inverse problem, e.g., unique reconstruction of the permanent charge density as a function of space (as we shall see below).

3.2. Design. The general remarks and notation of section 3.1 are also valid here. However, in the case of (optimal) design, there is an objective to be achieved instead of an object to be determined. In the applications to ion channels we have in mind, the primary objective is always to increase selectivity of one species over another. As discussed in detail in [GE02], selectivity has to be defined by experimental

results, and several different selectivity measures are available. A selectivity measure S_j of a species can be defined as a functional of ion densities and fluxes (possibly at varying voltage; cf. [GE02]). Since the densities and fluxes depend implicitly on the unknowns P related to the permanent charge (total number of charges or the constraining potential), the selectivity measure can also be rewritten as a functional $S_j = S_j(P)$ of these parameters. If the aim is to increase selectivity of species a over b , then one can minimize a relative selectivity measure

$$(3.3) \quad Q(S_a(P), S_b(P)) \rightarrow \min_P.$$

A simple widely used choice which we also use in our computational experiments is the selectivity quotient $Q(S_a, S_b) = -\frac{S_a}{S_b}$ (note that minimizing the negative quotient is equivalent to the original aim of maximizing the relative sensitivity). Analogous treatment is possible for other choices of Q , e.g., $Q(S_a, S_b) = \frac{S_b}{S_a}$ or $Q(S_a, S_b) = -S_a + S_b$.

In practice, to achieve a design task does not mean to actually maximize the functional Q , but usually one is satisfied if a significant improvement with respect to the criterion described by Q , e.g., the channel selectivity, is achieved.

The optimal design problem shares many of the problems of instability and ill-posedness with the identification problem. In the optimal design problem, however, there are no input data, but only a goal to be achieved, so that noise in the input data is not relevant. However, if one minimizes a functional Q as part of the solution of the design problem, as was done previously in the identification problem, then first of all the minimizer might not exist, which means that the norm of P tends to infinity in the associated minimization algorithm. Even if a minimizer exists, it might not be robust with respect to small perturbations of the problem (modeling errors, numerical errors, small changes of applied voltage and concentrations, etc.), so that a computed solution becomes useless in practice. Due to these instabilities, we have used regularization approaches to solve the design problem similar to those used for the identification problem (section 5).

We finally mention that optimal design problems for PNP systems have also been investigated before in semiconductor applications (cf. [HP02a, HP02b, BP03]), but again there are many significant differences in applications to ion channels. Besides all the differences in the forward problem, the optimal design of semiconductors (and, in particular, the objective functional) is always related to currents. In semiconductors, only holes and electrons carry charge, and so there is no analogue to selectivity measures of ion channels. Hence, the optimal design task for ion channels is a quite new problem that connects only loosely to previous literature.

4. Analysis of a simplified model. In order to obtain further insight into the structure of the inverse problems, we study a simplified model case for a spatially one-dimensional setup, i.e., $\Omega = (-L, L)$, with the channel being the subregion $(-\ell, \ell)$. We ignore all direct interactions; i.e., we set $E^{ex} \equiv 0$, and, moreover, we set $\mu_k^0 \equiv 0$. Hence, we arrive at the one-dimensional PNP model

$$(4.1) \quad -\lambda^2 V'' - \sum_{j=1}^M z_j \rho_j = 0,$$

$$(4.2) \quad J'_k = 0, \quad k = 1, \dots, M-1,$$

$$(4.3) \quad J_k - \rho_k z_k V' - c_k \rho_k' = 0, \quad k = 1, \dots, M-1,$$

with boundary conditions

$$V(-L) = 0, \quad V(L) = U, \quad \rho_k(\pm L) = \eta_k^\pm, \quad k = 1, \dots, M - 1.$$

The equations simplify after an exponential transform to a new set of variables (also called *Slotboom variables*; cf. [MRS90]) $u_k = e^{-\beta_k V} \rho_k$, where $\beta_k = -\frac{z_k}{c_k}$. We obtain

$$(4.4) \quad -\lambda^2 V'' - \sum_{j=1}^{M-1} z_j e^{\beta_j V} u_k = z_M \rho_M,$$

$$(4.5) \quad J'_k = 0, \quad k = 1, \dots, M - 1,$$

$$(4.6) \quad J_k - c_k e^{\beta_k V} u'_k = 0, \quad k = 1, \dots, M - 1,$$

with boundary values $V(-L) = 0, V(L) = U, u_k(-L) = \eta_k^-,$ and $u_k(L) = e^{-\beta_k U} \eta_k^+.$ Starting from this transformation, (4.5) and (4.6) can be integrated to obtain the solution

$$(4.7) \quad \rho_k(x) = \left(\eta_k^- + (e^{-\beta_k U} \eta_k^+ - \eta_k^-) \frac{G_k(x)}{G_k(L)} \right) e^{\beta_k V(x)}$$

with the function

$$G_k(y) := \int_{-L}^y e^{-\beta_k V(x)} dx.$$

Inserting the explicit solution for the concentrations from the NP equations into the Poisson equation, we obtain a single nonlinear integro-differential equation for the electric potential as

$$(4.8) \quad -\lambda^2 V'' - \sum_{k=1}^{M-1} \mathcal{R}_k[V] = z_M \rho_M$$

with the nonlinear operators \mathcal{R}_k given by

$$(4.9) \quad \mathcal{R}_k[V](x) = z_k \left(\eta_k^- + (e^{-\beta_k U} \eta_k^+ - \eta_k^-) \frac{G_k(x)}{G_k(L)} \right) e^{\beta_k V(x)}.$$

The fluxes J_k can be computed as

$$(4.10) \quad J_k = \frac{(e^{-\beta_k U} \eta_k^+ - \eta_k^-)}{\int_{-L}^L e^{-\beta_k V(x)} dx}.$$

Since the fluxes J_k are constant in spatial dimension one (and $J_M = 0$), we obtain the current globally as

$$(4.11) \quad I = \sum_{k=1}^{M-1} z_k J_k.$$

From a computational viewpoint, it seems attractive to consider a setup around (thermodynamic) equilibrium, since the solution of the forward model can be approximated by the simpler linearization around the equilibrium state. An equilibrium situation is obtained if the fluxes of all species vanish, which means in the one-dimensional

setting that $\eta_k^- = e^{-\beta_k U} \eta_k^+$, since the flux of every ionic species vanishes in this case. Note that one can always find suitable combinations of the bath concentrations that satisfy the above equilibrium condition as well as charge neutrality (e.g., vanishing bath concentration will always be an equilibrium case), so that we obtain a family of equilibria, still freely parameterized by the voltage U . This is an important particular feature of PNP systems in channels and will allow us to study some new effects. On the other hand, this also highlights possible redundancy in the data, since there are several parameter combinations that produce zero fluxes and even more that produce zero current, i.e., data without information content for the inverse problem.

The equilibrium electric potential parameterized by U will satisfy

$$(4.12) \quad -\lambda^2 V''_{0,U} - \sum_{k=1}^{M-1} z_k \eta_k^- e^{\beta_k V_{0,U}} = z_M \rho_M, \quad V_{0,U}(-L) = 0, V_{0,U}(L) = U.$$

Since β_k and $-z_k$ have the same sign and since η_k^- is nonnegative, the nonlinear terms $z_k \eta_k^- e^{\beta_k V_{0,U}}$ in the Poisson equation depend monotonically on $V_{0,U}$, so that the existence and uniqueness of the solution can be seen easily, as well as the stable dependence on ρ_M .

Now consider the linearization of the problem around the equilibrium values of η_k^\pm , i.e., the first-order change (in ϵ) of the output I with respect to perturbations of the form $\eta_k^\pm + \epsilon \hat{\eta}_k^\pm$ that still satisfy charge neutrality. The first-order expansion of the integral term in (4.10) disappears, since the numerator vanishes at equilibrium, and hence the linearized output is given by

$$\hat{I}(U) = \sum_{k=1}^{M-1} z_k \frac{(e^{-\beta_k U} \hat{\eta}_k^+ - \hat{\eta}_k^-)}{\int_{-L}^L e^{-\beta_k V_{0,U}(x)} dx}.$$

We mention that the use of \hat{I}_U instead of I produces only a restriction of the data set. It is not a simplifying assumption because \hat{I}_U can be computed from the measurements of currents I in a full range of parameters around their equilibrium values.

Now assume that $M \geq 4$, so that we have at least three different mobile species. Then one can always find values $\hat{\eta}_k^\pm$ satisfying charge neutrality such that $\hat{\eta}_k^- = e^{-\beta_k U} \hat{\eta}_k^+$, $k \neq m$, and $\hat{\eta}_m^- \neq e^{-\beta_m U} \hat{\eta}_m^+$ for some $m \in 1, \dots, M - 1$. Hence, for this choice,

$$\hat{I}(U) = z_m \frac{(e^{-\beta_m U} \hat{\eta}_m^+ - \hat{\eta}_m^-)}{\int_{-L}^L e^{-\beta_m V_{0,U}(x)} dx},$$

and therefore one can directly infer the knowledge of $M(U) = \int_{-L}^L e^{-\beta_m V_{0,U}(x)} dx$ from the knowledge of \hat{I}_U . Since the equilibrium Poisson equation can be solved uniquely for fixed U and given ρ_M , the forward map can be related to a (nonlinear) integral operator, and the identification of the permanent charge density corresponds to a nonlinear integral equation of the first kind (the unknown appears only under the integral sign), which is a classical ill-posed problem (cf. [En97, Gr84]).

The analysis particularly simplifies for the equilibrium case of small bath concentrations, i.e., a perturbation of $\eta_k^\pm \equiv 0$. In this situation, we can compute $V_{0,U} = V_{0,0} + \frac{x \pm L}{2L} U$, where $V_{0,0}$ solves

$$-\lambda^2 V''_{0,0} = z_M \rho_M, \quad V_{0,0}(\pm L) = 0.$$

Noticing that there is a one-to-one dependence between ρ_M and the function $f := e^{-\beta_m V_{0,0}}$, we can rephrase the integral equation as

$$\tilde{M}(\sigma) = \int_{-L}^L e^{-\sigma x} f(x) \, dx$$

with $\tilde{M}(\sigma) = e^{\frac{\beta_m U}{2}} M(U)$ and $\sigma = -\frac{\beta_m}{2L} U$. Varying the voltage U in an interval $(-U_{max}, U_{max})$ is then equivalent to varying $\sigma \in (-\sigma_{max}, \sigma_{max})$. Hence, we arrive at a Fredholm integral equation of the first kind for f , with an analytic kernel, a problem which is known to be severely ill-posed (see the analysis below). The standard classification of ill-posedness we refer to divides into mildly ill-posed problems with an error amplification that grows like a polynomial with increasing frequency and severely ill-posed problems with faster growing error amplification (usually exponentially). The remaining step of computing ρ_M from f is another nonlinear ill-posed problem, which involves the application of a logarithm and two differentiations to compute

$$\rho_M = \frac{\lambda^2}{z_M \beta_m} (\log f)''$$

and is therefore mildly ill-posed.

Identifiability, i.e., uniqueness of the reconstruction from the given data set, can be guaranteed in this case independent of the size of U_{max} (respectively, σ_{max}). Assume that $M(\sigma)$ is known in an arbitrarily small interval around $\sigma = 0$; then, in particular, all derivatives

$$(-1)^p \frac{d^p}{d\sigma^p} \tilde{M}(0) = \int_{-L}^L x^p f(x) \, dx, \quad p = 0, 1, \dots,$$

and hence all moments of f are known. Since a function is uniquely determined from its moments, we conclude the uniqueness of the reconstruction of f and subsequently of ρ_M . Note that we have used only a subset of the data to show identifiability, and so one might argue that the full inverse problem is actually overdetermined.

In order to gain some quantitative information about the instability present in the identification problem, we investigate the singular values of the operator

$$K : L^2([-L, L]) \rightarrow L^2([-\sigma_{max}, \sigma_{max}]), \quad f \mapsto \int_{-L}^L e^{-\sigma x} f(x) \, dx.$$

Note that K is a symmetric positive semidefinite operator, and hence the singular values and eigenvalues are equal. As mentioned above, the fact that the integral kernel is analytic implies that the eigenvalues decay faster than any polynomial (cf. [We68]). One actually expects exponential decay. This is confirmed by a numerical computation of the spectrum (with 1025 grid points) displayed in Figure 2, where we plot the singular values (rescaled so that the leading one is equal to one) for different values of σ_{max} and $L = 1$ fixed. (We do not consider the change of L , since its change can be related to the change of σ_{max} by a simple rescaling.) Since the error amplification factor at each frequency equals the inverse of the singular value, this problem is indeed severely ill-posed. The influence of the maximal value σ_{max} is seen by comparing the four results in the figure. For a smaller value of σ_{max} , the decay of singular values is faster, which implies a more significant loss of information. Since σ_{max} is proportional to the maximal value of the applied voltage U , this result shows that one should make measurements at as large a voltage as possible to reduce the instability in the reconstruction as much as possible.

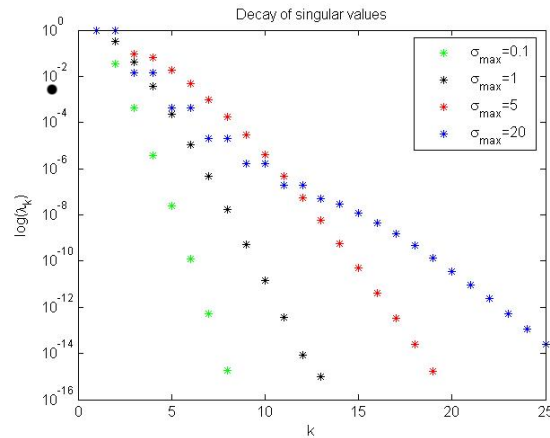


FIG. 2. Leading singular values of the linear operators K for different values of σ_{max} .

5. The full inverse problems. In the following, we shall discuss the *forward problem*, namely the solution of the PNP-DFT model for given data, and the map F to the output, namely current-voltage curves for different bath concentrations. This map will be of fundamental use in the mathematical formulation and solution of the inverse problems. As a first step, we analyze the existence and uniqueness of solutions, which hold at least for small bath concentrations of the free species.

5.1. Properties of the forward operators. In the following, we provide an analysis of the PNP model, including the excess free energy. We mention that an extensive analysis of PNP systems is available for applications to semiconductor devices (cf. [MRS90] and the references therein), but the inclusion of the excess free energy in the ion channel model prevents a direct extension of these available results. We shall consider only a particular case of small bath concentrations in the following, in order to make sure that the forward operator can indeed be well-defined at least in some parameter range. To clarify, we state the system we consider, namely the solution of (2.1), (2.10) and, as an equivalent statement of (2.2),

$$(5.1) \quad \nabla \cdot J_k = 0, \quad k = 1, \dots, M,$$

together with (2.6) and (2.8). In order to show the specific dependence on the applied voltage U , the vector of bath concentrations $\eta = (\eta_k)_{k=1, \dots, M-1}$, the number N_M of confined particles, and the confining potential μ_M^0 , we introduce the following nomenclature:

We denote by $\mathcal{P}(U, \eta; N_M, \mu_M^0)$ the problem of solving (2.1), (2.10), (5.1), (2.6), (2.8) for the unknowns $(V, \rho_1, \dots, \rho_M)$.

We shall assume that $U \in H^{\frac{1}{2}}(\partial\Omega_D) \cap L^\infty(\Omega_D)$ and that E^{ex} is twice continuously differentiable on $H^1(\Omega)^M \cap L^\infty(\Omega)^M$. For the sake of simplicity, we also assume that $E^{ex}(\rho_1, \dots, \rho_{M-1}, \cdot)$ is a convex functional of the last variable if $\rho_k, k = 1, \dots, M-1$, is sufficiently small. Consequently, the map between the density ρ_M and the confining potential μ_M^0 is monotone in this range.

We start our analysis in the case of zero bath concentrations, i.e., $\eta_k = 0$, for $k = 1, \dots, M-1$. In this case, there is obviously no flow, and we can easily construct a solution.

LEMMA 5.1. *Under the above assumptions, there exists a solution*

$$(V, \rho_1, \dots, \rho_M) \in H^1(\Omega)^{M+1} \cap L^\infty(\Omega)^{M+1}$$

of problem $\mathcal{P}(U, 0; N_M, \mu_M^0)$, which satisfies $\rho_k \equiv 0$ for $k = 1, \dots, M - 1$.

Proof. The functions $\rho_k \equiv 0$ satisfy the boundary conditions as well as (2.10), (5.1). We now look for a solution of the remaining problem

$$-\lambda^2 \Delta V = z_M \rho_M, \quad \rho_M = \gamma_M N_M \exp\left(-\frac{z_M V + \mu_M^0 + \mu_M^{ex}}{c_M}\right),$$

with the boundary conditions remaining for ρ_M and V . Using the monotone dependence of μ_M^{ex} on ρ_M it is straightforward to show that for each $V \in H^1(\Omega) \cap L^\infty(\Omega)$ there exists a unique solution $\rho_M \in H^1(\Omega) \cap L^\infty(\Omega)$ of the second equation. Moreover, the specific exponential dependence on V implies that the map $\mathcal{F} : V \mapsto -z_M \rho_M$ is monotone and continuously Fréchet-differentiable, too. Hence, we can perform a further reduction to a problem of the form

$$-\lambda^2 \Delta V + \mathcal{F}(V) = 0 \quad \text{in } \Omega$$

with Neumann and Dirichlet boundary conditions on the respective parts of $\partial\Omega$. Finally, a standard result for elliptic equations with monotone operators implies existence and uniqueness of this remaining problem (cf. [Sh96]). \square

In order to proceed to small positive bath concentrations, we shall perform a linearization around zero concentrations. The formal linearization of the PNP system around a given state $(V, \rho_1, \dots, \rho_M)$ is given by

$$(5.2) \quad -\lambda^2 \Delta \hat{V} - \sum z_k \hat{\rho}_k = f_0,$$

$$(5.3) \quad \nabla \cdot \left(c_k \nabla \hat{\rho}_k + z_k \rho_k \nabla \hat{V} + z_k \rho_k \nabla \left(\sum_j \frac{\partial \mu_k^{ex}}{\partial \rho_j} \hat{\rho}_j \right) + z_k \hat{\rho}_k \nabla (V + \mu_k^0 + \mu_k^{ex}) \right) = \nabla \cdot (\rho_k \nabla f_k),$$

$$(5.4) \quad c_M \frac{\hat{\rho}_M}{\rho_M} + \hat{V} + \sum_j \frac{\partial \mu_M^{ex}}{\partial \rho_j} \hat{\rho}_j = f_M$$

with right-hand sides $f_j \in L^\infty(\Omega) \cap H^1(\Omega)$, $j = 0, \dots, M$, to be solved for \hat{V} and $\hat{\rho}_k$. The left-hand side of (5.2), (5.3) is indeed a Fréchet derivative of the left-hand side in the PNP system. We are going to prove that this linearization defines a continuously invertible linear operator $(f_0, \dots, f_M) \mapsto (\hat{V}, \hat{\rho}_1, \dots, \hat{\rho}_M)$ around zero bath concentrations, i.e., for $(V, \rho_1, \dots, \rho_M)$ being the solution of problem $\mathcal{P}(U, 0; N_M, \mu_M^0)$ from Lemma 5.1. The implicit function theorem in Banach spaces (cf. [De85, Theorem 15.1]) then yields the local existence and uniqueness of solutions as well as the well-posedness of the linearized problems for small bath concentrations.

LEMMA 5.2. *Let $(V, \rho_1, \dots, \rho_M)$ be the solution of problem $\mathcal{P}(U, 0; N_M, \mu_M^0)$, as in Lemma 5.1. Then, for any $f_j \in L^\infty(\Omega) \cap H^1(\Omega), \dots$, there exists a unique solution*

$$(\hat{V}, \hat{\rho}_1, \dots, \hat{\rho}_M) \in H^1(\Omega)^{M+1} \cap L^\infty(\Omega)^{M+1}$$

of (5.2), (5.3), which depends continuously on the data.

Proof. Due to $\rho_k \equiv 0$ for $k = 1, \dots, M - 1$, the NP equations (2.2) simplify to

$$\nabla \cdot (c_k \nabla \hat{\rho}_k + z_k \hat{\rho}_k \nabla (V + \mu_k^0 + \mu_k^{ex})) = 0$$

and, in particular, become scalar equations decoupled from the other variables. After a change of variables to $u_k := \hat{\rho}_k \exp(-\beta_k(V + \mu_k^0 + \mu_k^{ex}))$, with $\beta_k = -\frac{z_k}{c_k}$, we obtain the equation

$$\nabla \cdot (c_k \exp(-\beta_k(V + \mu_k^0 + \mu_k^{ex})) \nabla u_k) = 0,$$

whose well-posedness can be analyzed by standard techniques for elliptic equations due to the absence of convective terms. Using also the equilibrium boundary conditions for $\hat{\rho}_M$, we obtain the remaining problem

$$-\lambda^2 \Delta \hat{V} - z_M \hat{\rho}_M = \tilde{f}_0, \quad c_M \frac{\hat{\rho}_M}{\rho_M} + \hat{V} + \frac{\partial \mu_M^{ex}}{\partial \rho_M} \hat{\rho}_M = \tilde{f}_M,$$

now with the given right-hand sides $\tilde{f}_0 = \sum_{k=1}^{M-1} z_k \hat{\rho}_k + f_0$ and $\tilde{f}_M = \sum_{k=1}^{M-1} (f_k - \frac{\partial \mu_M^{ex}}{\partial \rho_k} \hat{\rho}_k)$. For the remaining problem to compute \hat{V} and $\hat{\rho}_M$, exactly the same arguments as in Lemma 5.1 apply, so that we can conclude the well-posedness of the linearization. \square

We now have collected the necessary prerequisites to prove the well-posedness of the problem for small bath concentrations.

THEOREM 5.3. *Let $\|\eta_k\|_{H^{1/2}(\Gamma_D)}$ and $\|\eta_k\|_{L^\infty(\Gamma_D)}$ be sufficiently small. Then, for each $U \in H^{1/2}(\Gamma_D)$, there exists a locally unique solution*

$$(V, \rho_1, \dots, \rho_M) \in H^1(\Omega)^{M+1} \cap L^\infty(\Omega)^{M+1}$$

of problem $\mathcal{P}(U, \eta; N_M, \mu_M^0)$, and the linearized problem (5.2), (5.3) is well-posed.

Proof. In the lemmas above, we have shown that the problem for $\eta \equiv 0$ is well-posed and its Fréchet-derivative exists with continuous inverse in the respective function spaces. Moreover, the equation operator is Fréchet differentiable, so that we can apply the implicit function theorem in Banach spaces (cf. [De85, Theorem 15.1]) to conclude that a locally unique solution of problem $\mathcal{P}(U, \eta; N_M, \mu_M^0)$ exists around $\eta \equiv 0$ and that the linearized problems are well-posed for small η . \square

As a direct consequence of the above result, we can verify the well-definedness and even differentiability of the map from the relevant input data related to the permanent charge to the output current.

COROLLARY 5.4. *Let $\|\eta_k\|_{H^{1/2}(\Gamma_D)}$ and $\|\eta_k\|_{L^\infty(\Gamma_D)}$ be sufficiently small. Then, for each $U \in H^{1/2}(\Gamma_D)$, the map*

$$(5.5) \quad \begin{aligned} G(\cdot; U, \eta) : \mathbb{R}^+ \times (H^1(\Omega) \cap L^\infty(\Omega)) &\rightarrow \mathbb{R}, \\ (N_M, \mu_M^0) &\mapsto I(U, \eta) = \int_{\Gamma_D} \sum z_k J_k \, d\sigma \end{aligned}$$

is well-defined, compact, and continuously Fréchet differentiable.

5.2. Regularization. In practice, one has to discretize the function I of the bath concentrations and voltages, so that one computes only a finite number K of function evaluations, denoted by I_1, \dots, I_K , and the operator F can be written in the form $F = (F_1, \dots, F_K)$. The evaluation of a single part F_j amounts to a single solution of the forward problem for a specific combination of the bath concentrations and the applied voltage and the subsequent computation of the outflow current from the solution. The linearization is then of the form $F' = (F'_1, \dots, F'_K)$, and its adjoint is of the form $F'(P)^* = \sum_{j=1}^K F'_j(P)^*$. Note that the operators F_j are of the form $F_j(P) =$

$G(H(P); U^j, \eta^j)$, where H is the affine linear operator mapping the parameter P to the pair (N_M, μ_0^M) . If both N_M and μ_0^M are the unknowns in the inverse problem, then H is just the identity. If one of them is known, then H is the operator mapping the other one to the pair (N_M, μ_0^M) . The well-definedness and compactness of the operators F_j and subsequently of F can directly be inferred from Corollary 5.4, and one can even conclude the existence of Fréchet derivatives of F .

Due to the instability of the inverse problems, regularization methods should be used for their solution. One of the most frequently used classes of regularization methods for nonlinear problems is variational methods (cf. [EHN96, EKN89, SV89]), where the inverse problem (3.2) is approximated by the variational problem

$$(5.6) \quad J_\alpha(P) := \|F(P) - I^\delta\|^2 + \alpha R(P) \rightarrow \min_P$$

with a suitable regularization functional R (e.g., $R(P) = \|P - P^*\|^2$ for Tikhonov regularization) and a positive real regularization parameter α . An alternative is iterative regularization methods (cf. [KNS06, ES00, OBGXY05]), based on an iteration procedure of the form

$$(5.7) \quad P_{n+1} = P_n - G_n(F(P_n) - I^\delta)$$

with a linear or even nonlinear operator G_n (depending on P_n in general). Such an iterative scheme becomes a regularization method with the appropriate choice of a stopping index n_* at which the iteration is stopped. A common choice of stopping rule—due to its computational simplicity—is the discrepancy principle; i.e., the iteration is stopped when the residual reaches the order of the noise level. We mention that with the properties of the operator F and its linearization F' derived above, the existing theory of variational and iterative regularization methods can be applied (cf. [EHN96, EKN89, KNS06, ES00]) to our case. We can then guarantee the regularizing properties and convergence of the methods we apply to inverse problems in ion channels.

We mention that an analogous iteration method to (5.7) can (and should) be used to solve the variational problem appearing in variational methods. In our test examples detailed below, we carried out a gradient-based method, which is an iteration procedure of the form

$$(5.8) \quad P_{n+1} = P_n - \tau_n [F'(P_n)^*(F(P_n) - I^\delta) + \alpha R'(P_n)] = P_n - \tau_n J'_\alpha(P_n)$$

which can be interpreted as a minimization method for the variational problem (5.6) or, with $\alpha = 0$ and an appropriate choice of the stopping index, as an iterative regularization method of the form (5.7). Here F' , R' denote the derivatives of the operator F and the functional R , respectively, in the appropriate function spaces. Moreover, $F'(P_n)^*$ is the adjoint of the derivative (which is a linear operator between these function spaces).

The simplest, but already quite significant, inverse problem to be solved in this context is to determine the number N_M , characterizing the total permanent charge (i.e., $P = N_M$ in the above setting). As noticed above, this problem is one-dimensional as an inverse problem (although, of course, the direct problem is still a system of partial differential equations), and hence the instability does not appear. Also, this problem is *not* very challenging with respect to the optimization algorithm, which is fortunate because this problem is particularly important biologically. The main issue in the optimization is the evaluation of the functional J_α (respectively, the operator

F) and its derivative, which involves the solution of several forward problems. The derivatives can be computed via the adjoint operator $F'_j(P_n)^*$ or approximated simply by finite differencing, which typically creates a higher computational effort but needs no further implementations than those already used to evaluate the forward operator. Since the aim is to identify a single real number only, it seems reasonable that this is possible for rather low values of K , and indeed our computational experiments indicate that this is possible with high accuracy already for $K = 10$ and even for $K = 5$.

The next level of complexity is the identification of the confining potential μ_M^0 or the identification of the permanent charge ρ_M . By analogy to the simplified problems considered above, we have to expect that these identifications are severely ill-posed so that regularization is of fundamental importance. The computational complexity of this inverse problem is much higher also because a much higher number K of different setups is needed in order to obtain a reasonable reconstruction of the confining potential or the permanent charge density. It is interesting that numerical exploration of the forward problem suggests that the details of the distribution of permanent charge, and thus the details of the constraining potential, are much less important for biological function than the total amount of that charge as long as the charge is of one sign and also is not too small.

Also for the design tasks introduced above, one can define variational regularization methods by just changing the objective functional to $Q + \alpha R$. In our computational tests, we specifically use a variational method of the form

$$(5.9) \quad Q(S_a(P), S_b(P)) + \alpha \|P - P^*\|^2 \rightarrow \min_P,$$

where P^* is a favored initial design. In a synthetic ion channel, this a priori guess could introduce additional criteria into the minimization; e.g., P^* can represent a total charge or a confining potential that is easy to manufacture, so that the regularization term would introduce a criterion for the minimizer to be close to easily manufacturable states. In this way, robustness is introduced in the problem, which can also be observed in the results of our computational experiments.

From a computational viewpoint, the minimization of the regularized variational problem (5.9) is an analogous task to the one appearing in identification problems. The main steps are the evaluation of the objective functional (by solving forward problems and subsequently evaluating selectivity measures) and the computations of gradients of the objective functional with respect to P . The latter task can again be carried out by finite differencing, which reduces to additional solves of the forward problem and creates a high computational effort, or by solving appropriate adjoint problems. The total computational effort for solving optimal design problems is usually much less than for solving identification problems, since the selectivity measure is computed only for very few different combinations of bath concentrations and voltages. Significantly fewer forward problems have to be solved for evaluating the objective functional than in the case of identification.

6. Case study: An L-type Ca channel. In this section, we report on a case study performed for an L-type Ca channel (LCC), for which we performed the identification and design tasks as described above. A sketch of the LCC is provided in Figure 3.

We choose the LCC because it is of enormous importance as the regulator of the contraction of skeletal and cardiac muscle, and it has received extensive attention in

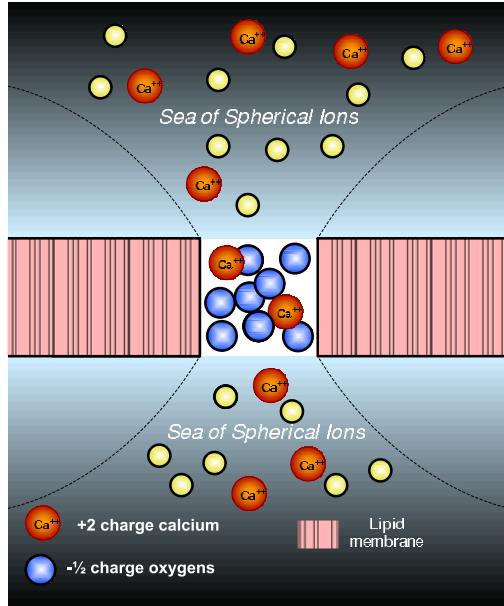


FIG. 3. Illustration of the LCC when filled with Ca.

TABLE 1

Parameter settings for the LCC example, using elementary charge $e = 1.602 \times 10^{-19} C$.

k	1	2	3	4	5
Species	Ca^{2+}	Na^+	Cl^{-1}	H_2O	$O^{-1/2}$
Charge z_k	$2e$	e	$-e$	0	$-\frac{e}{2}$
$\rho_k(L)$	6 mM	12 mM	24 mM	55 M	0 M
$\rho_k(-L)$	var	var	var	55 M	0 M

the biophysics literature for that reason (cf., e.g., [KMS83, Hetal92, SMC03]). Recent work shows quite clearly that many properties of two types of calcium channels can be quantitatively described by extended versions of the PNP model (cf. [Betal06, GNE02, Mietal06, Mietal04, Waetal05, XWGM06]). Given the importance of calcium channels and the demonstrated ability of PNP-type models to explain current voltage relations and selectivity over large ranges of concentration of many types of ions, it is natural to use this system in our investigation of inverse problems.

6.1. Forward model. The forward model of the LCC involves the electrical potential V and five densities ρ_k modeling the three mobile ion species Ca^{2+} , Na^+ , Cl^- , a neutral mobile species H_2O , and half-charged oxygens $O^{-1/2}$ corresponding to the permanent charge. This means that each forward problem consists of a coupled system of six partial differential equations, the Poisson equation (2.1) and five NP equations (2.2) for the densities ρ_1, \dots, ρ_5 (see Table 1 for the assignment of densities to the species).

The channel is modeled as cylindrical with diameter 0.4 nm ($y - z$ plane) and length $2\ell = 1$ nm (x -direction), embedded in two baths both of length 1.7 nm. This yields a total length of 4.4 nm for the system, and therefore the computational domain is chosen as $(-L, L)$ with $L = 2.2$ nm.

From the geometry of the system, it is rather obvious that the flow arises in

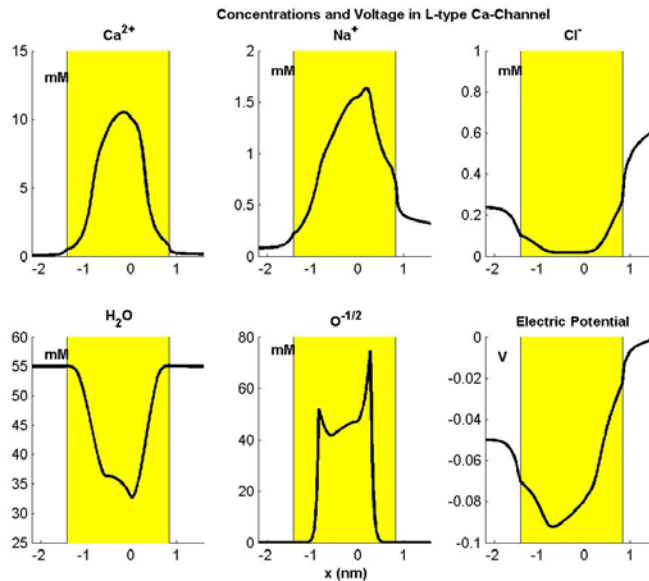


FIG. 4. Plot of ion densities and electr potential as functions of spatial location for an LCC with applied voltage 50 mV. The illuminated region is the channel which is scaled in the x -direction by a factor five compared to the bath regions.

the x -direction, and the model can be reduced by averaging in the $y - z$ plane to a one-dimensional problem with single spatial variable x ; but note that our procedures are in no way restricted to the one-dimensional case. In this averaging procedure, the shape of the channel has to be taken into account, which yields some spatially dependent coefficients in the reduced system of one-dimensional differential equations. The details of the averaging and an exact statement of the equations to be solved for the LCC can be found in [GNE02, GNE03, NCE00, BEE06].

We solve the forward problem on a grid with $n = 1251$ (for data generation) and $n = 1000$ cells (for the inverse problem) with a standard conforming finite element discretization of the electric potential and the Poisson equation and a mixed finite element discretization of the continuity equations for the ions. Since we have the electric potential and five different species (Ca^{2+} , Na^+ , Cl^- , H_2O , and $\text{O}^{-1/2}$), this yields $1252 + 5 \times 1251 = 7507$ degrees of freedom (for data generation), respectively, $1001 + 5 \times 1000 = 6001$ (for the inverse problem) degrees of freedom, in the forward problem.

The measurements are the currents, taken as functions of the voltage and of the left bath concentrations $\rho_k(-L)$ for $k = 1, 2$, whereas the right bath concentrations $\rho_k(L)$ are kept fixed. The water concentration (“osmolarity”) is fixed in both baths, and $\rho_5(\pm L) = 0$, because of the confinement of permanent charge to the channel. The concentrations $\rho_3(\pm L)$ are finally determined from the charge neutrality $\sum_k z_k \rho_k(\pm L) = 0$. The parameter settings for the boundary values are given in Table 1, where var means that the values are varied in the identification process.

The solution of the forward model for an LCC with the above settings—applied voltage $U = 50$ mV, $N_M = 8$ confined oxygens, and confining potential μ_M^0 plotted as the exact value in Figure 8—is illustrated in Figure 4. The illuminated region corre-

sponds to the channel, while the white region to the left and right correspond to the bath. In this example, one observes many typical effects, in particular the selectivity properties of the channel. Due to the negative permanent charge (oxygen), there is an attractive electrical force on the positively charged ions (Na and Ca) and a repulsive force on the negatively charged ions (Cl). Moreover, the additional “chemical” forces arising from the finite volume of the ions produce an additional decrease of the densities in the channel region. These excluded volume forces are particularly important because of the narrow cross section of the channel. This decrease in densities can be observed in particular in the plot of the water density, since it is the only force acting on this species. (There are no electrical interactions with water in our system due to neutrality of our model of water.)

6.2. Identification I: Reconstruction of the total charge. In this case, one assumes that the structure of the channel is known, but the total charge of the crowded elements in the selectivity filter is unknown. The inverse identification problem consists of identifying the total charge based on measurements of the total current for different bath concentrations of the ions. As noticed before, the reconstruction of the total charge is the simplest case of an inverse problem for ion channels, so that we expect more accurate results than for the more complicated inverse problems in the sections below.

This inverse problem is a finite-dimensional one. We try only to identify a single real number from a finite number of measurements. As mentioned above, this inverse problem is not ill-posed in the classical sense of inverse problems theory, cf. [EHN96], because of the low dimension. The only possible instability is due to nonlinearity effects, but such effects seemed not to appear in the various computational tests.

For a test of the inverse problem technique, we generated synthetic data for the setup as used in the LCC [GNE03], i.e., a crowded charge consisting of eight half-charged oxygens. This means we solve the forward problem with the finer grid and then compute the resulting currents. Subsequently, we perturb the synthetic measurements by noise and use them as data to solve the inverse problem. (The same technique is also used for the other inverse problems below.) In this way, we have a known reference solution, and we can check to see if the algorithm yields reasonable reconstructions in a stable way.

The reconstructions are carried out by a gradient method for the associated least-squares functional describing the residual. The gradients are approximated by finite differences. This is for illustration only. More efficient ways are possible to approximate the gradient for this and related problems, e.g., via adjoint problems.

In this case, one obtains very accurate reconstructions of the exact total charge even for noisy data and even for a rather low number of measurements, allowing us to deal effectively with this quite significant biological problem. The pessimism of early analysis can be removed if the problem is posed with PNP equations and solved with the methods of inverse problems (cf. [At79, AJ78]); see below. A typical setup consists of three different applied voltages (0.1V, 0V, -0.1 V) and two different concentrations for Na and Ca (2 mM and 4 mM) in the left bath. With all combinations, this gives $3 \times 2 \times 2 = 12$ measured values; i.e., the problem is already overdetermined. An illustration of the reconstruction process in this situation is given in Figure 5. Here the reconstructed mass of the crowded particles (scaled by the mass of the eight half-charged oxygens in the real structure) are plotted versus the number of iterations in the optimization method. In this case, a standard stopping criterion would stop the calculation after some 90 to 100 iterations. (The reconstruction does not change

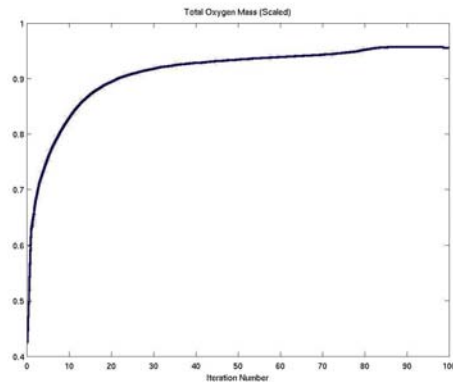


FIG. 5. Plot of the total charge (relative to the exact value) during the iterations of the gradient method.

significantly with more computation.) The difference between the scaled mass of the real total charge and the reconstructed one is less than 5%, although the initial value is quite far away from the solution. Similar behavior was found also in other tests with different initial values and parameter settings.

6.3. Identification II: Reconstruction of the structure. The second inverse problem is related to the reconstruction of the structure of the channel. This is done indirectly by identifying the confining potential acting on the crowded ions (oxygens in our example), which models the way the structure interacts with the channel. More specifically, the confining potential models the forces that keep the charged oxygens of the channel inside the selectivity filter.

The unknown in the above setting is given by $P = \mu_5^0$. Now the inverse problem is to find a space-dependent function on the channel region, which is really an infinite-dimensional problem. In an idealized setting, the unique reconstruction of the confining potential (as a function of space) would require an infinite number of measurements. Therefore, any measurement realized in practice (where, of course, only a finite number of measurements can be taken) has to be interpreted as a discretization of the problem with an infinite number of measurements. It therefore seems obvious that a higher number of measurements yields better reconstruction, and this is also confirmed by all our tests. On the other hand, a much higher number of measurements forces an extremely high computational effort.

The variation of the confining potential μ_5^0 has a significant influence only in the channel region, since outside it will just take some very large values that cause the confinement of the permanent charge species. In the solution of the identification problem, we use this a priori knowledge and approximate μ_5^0 by a constant function in the baths. Note that due to the large values of μ_5^0 in the bath regions, the concentration ρ_5 is almost zero there in any case.

As representative examples of the behavior of the reconstructions, we illustrate the results for

- (a) four applied voltages and different left bath concentrations for Na and Cl, for a total of $4 \times 2 \times 2 = 16$ measurements (voltages ± 10 mV, ± 5 mV and concentrations 2 mM, 4 mM),
- (b) six applied voltages and different left bath concentrations for Na and Cl, for

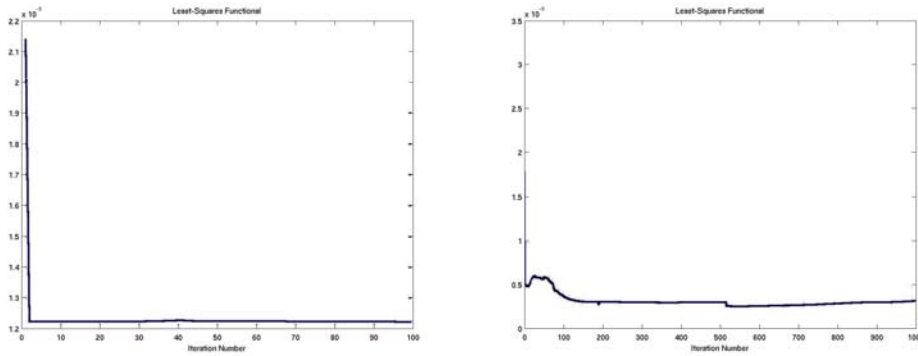


FIG. 6. Plot of the squared residual $\|F(P_n) - I^\delta\|^2$ as a function of the iteration number for $4 \times 2 \times 2$ measurements (left) and $6 \times 3 \times 3$ measurements (right).

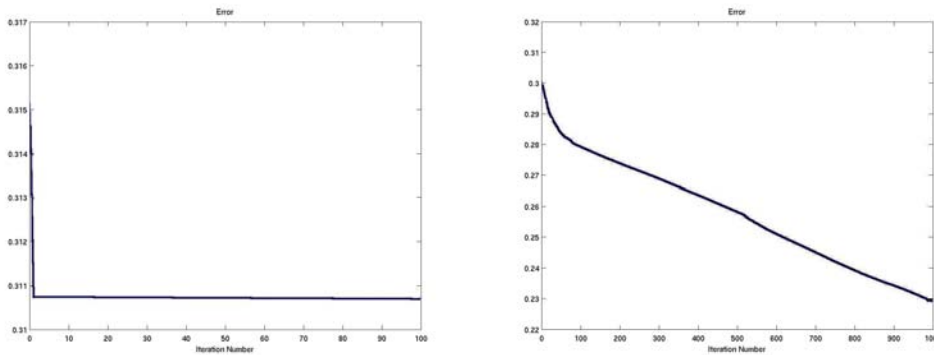


FIG. 7. Plot of the identification error $\|P_n - P^\dagger\|$ as a function of the iteration number for $4 \times 2 \times 2$ measurements (left) and $6 \times 3 \times 3$ measurements (right).

a total of $6 \times 3 \times 3 = 54$ measurements (voltages ± 10 mV, ± 6.6 mV, ± 3.3 mV and concentrations 2 mM, 4 mM, 6 mM), obtained with 0.1% noise. The resulting evolution of the least-squares functional during the iteration is plotted in Figure 6 (left for case (a) and right for case (b))—one observes that they are quite similar in the two cases, and the residual decreases to some value around the size of the noise level. As has to be expected for iterative regularization methods (cf. [EHN96, KNS06]), the evolution of the reconstruction error, however, is completely different, as one can see in the plots of Figure 7 (left for case (a) and right for case (b)). In the first case (16 measurements), the reconstruction error is hardly reduced, while in the second case, one already obtains a very significant decrease before the noise level is reached. This can also be seen from the final reconstructions obtained with a stopping of the iteration dependent on the noise, which are shown (here plotting the negative potentials for illustration purpose) in Figure 8 (left for case (a) and right for case (b)). The initial guess used in both cases is shown in Figure 9. One observes that the second reconstruction is already rather close to the real potential, in particular in the left part of the channel. The reason for the better reconstruction in the left part is that the concentrations are varied in the left bath, and so there is more sensitivity with respect to the data in this region.

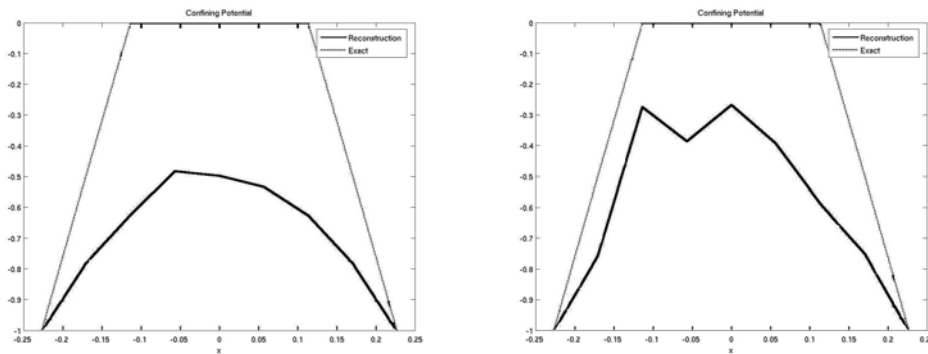


FIG. 8. Final reconstructions P_{n_*} obtained at the stopping index determined by the discrepancy principle for $4 \times 2 \times 2$ measurements (left) and $6 \times 3 \times 3$ measurements (right).

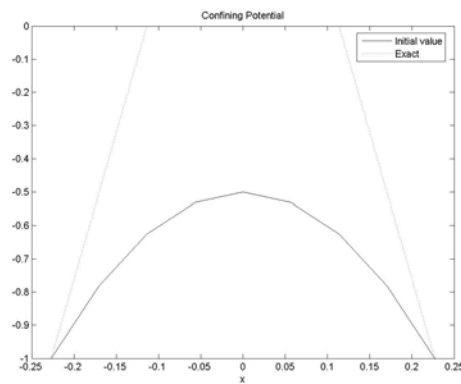


FIG. 9. Initial value P_0 used for all reconstructions of potentials.

These results clearly indicate that the reconstructions will improve for an increasing number of measurements. For a very high number of measurements, the computational complexity of the inverse problem dramatically increases and will be necessary to implement very efficient methods to compute reconstructions, including faster forward solvers (cf. [BW07]), adjoint methods for computing derivatives (cf. [GP00]), and multiscale versions of the regularization methods (cf. [Sch98, BM02]).

The instability of the identification problem in this case is illustrated in the plots of Figure 10. Here we use the same setup as before ($6 \times 3 \times 3$ measurements) but a slightly higher noise level (1%). We start with an initial guess where the residual is in the order of the noise level; in such a situation, a stopping rule for an iterative regularization such as the discrepancy principle would immediately stop the iteration. If one iterates further (which one would do when using a standard optimization stopping criterion based on the gradient of the residual), then the error starts to increase (and then possibly oscillates), although the residual is still decreasing. This situation is illustrated in Figure 10, where the least-squares functional and the error are plotted as functions of the iteration number. One observes that in this case the least-squares functional is still decreasing, but the error between the reconstruction and the exact solution can increase, which demonstrates the ill-posedness of the problem. Note that

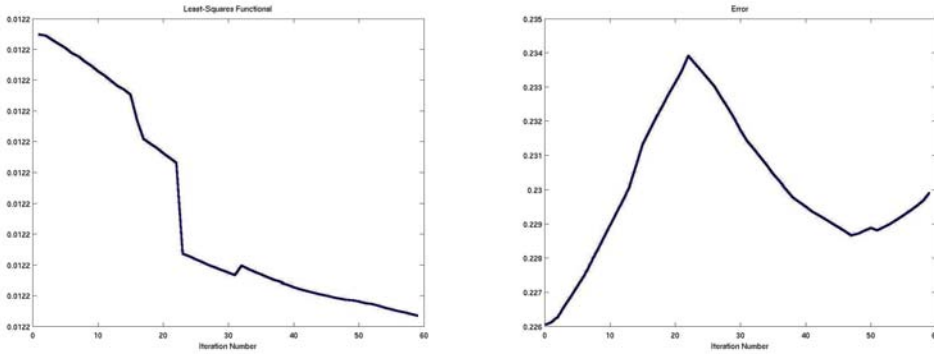


FIG. 10. Plot of the residual (left) and identification error $\|P_n - P^\dagger\|$ (right) as a function of the iteration number without regularizing stopping criterion.

this effect did not appear in the examples with a stopping criterion based on regularization theory as described in section 5, which again illustrates the importance of regularization.

6.4. Identification III: Reconstruction of the permanent charge density for PNP. As a final step in our study of identification problems, we consider the reconstruction of the permanent charge density ρ_M in a pure PNP model; i.e., the forward model consists in solving (2.1), (2.2), and (2.6) for $k = 1, \dots, M - 1$ with given ρ_M and $E^{ex} \equiv 0$. Apart from the elimination of the equation for ρ_M , the discretization and numerical schemes used to solve the PNP system are the same as in the previous section; in particular, we use the Landweber iteration as a regularization method.

In this case, we numerically implemented adjoint solvers to compute derivatives, which results in improved accuracy and lower computational effort even for finer discretizations (in this case, we use 21 grid points) of the unknown in the inverse problem. We refer the reader to [GP00] for a general overview of adjoint methodology and to [BEMP01, Wo06] for the derivation of adjoint problems in related semiconductor applications.

For the reconstruction, we used five different values of the voltage U and eight different bath concentrations of Na and Ca, which results in a total number of $5 \times 16 \times 16 = 1280$ measured values. With this amount of data, very reasonable reconstructions can be obtained even in the presence of noise. The development of the residual and error $\|P_n - P^\dagger\|$ are illustrated in Figures 11 (without noise) and 12 (with noise level 3%). One observes that the residual and error both decrease in a monotone way in the noiseless case, whereas a minimum of the error is reached after some iteration number in the presence of noise. However, at this iteration number the relative residual is already very close to the noise level, so that a stopping rule like the discrepancy principle would stop already slightly earlier. These results have been obtained with an initial value $P_0 \equiv 3$ and an exact value $P^\dagger \equiv 5$, but qualitatively similar results have been computed also with other choices of P_0 and P^\dagger .

The quality of the reconstructions is illustrated in Figure 13 for permanent charge P^\dagger being constant (left) and of a sinusoidal shape (right). In both cases, the starting value P_0 is dashed, the exact solution P^\dagger is dotted, and the reconstruction is the solid line. One observes that with the amount of data we use, it is possible to reconstruct the constant solution very accurately, while there remains some visible deviation for

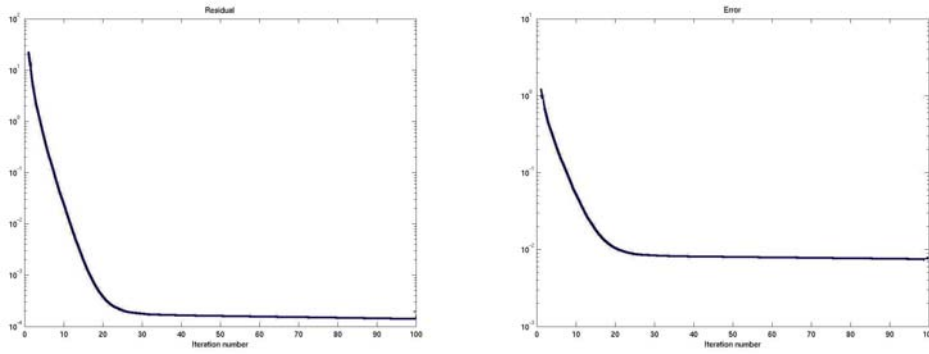


FIG. 11. Plot of the residual (left) and identification error $\|P_n - P^\dagger\|$ (right) as a function of the iteration number in the absence of noise.

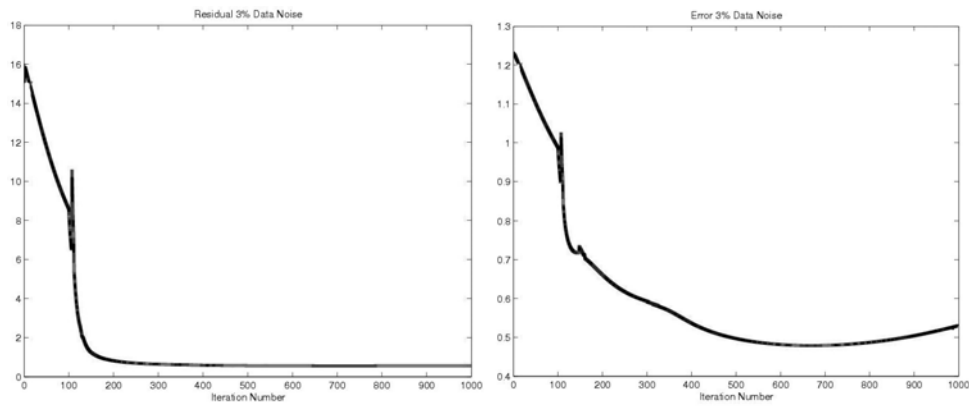


FIG. 12. Plot of the residual (left) and identification error $\|P_n - P^\dagger\|$ (right) as a function of the iteration number for 3% data noise.

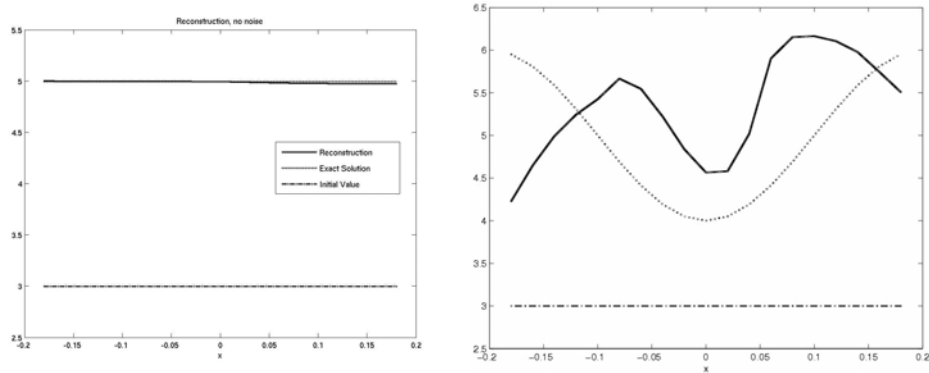


FIG. 13. Plot of reconstructions in the absence of noise for a spatially constant permanent charge (left) and a spatially varying permanent charge (right).

the more complicated shape. However, the magnitude of values as well as the principal shape (a valley in the middle) could also be reconstructed in the more difficult sinusoidal second case. Reconstructions of this moderate quality have to be expected in a severely ill-posed problem even for a larger number of measurements, and even these are quite tricky to achieve. Situations in which the permanent charge changes sign or reaches nearly zero are likely to pose even more problems.

6.5. Design: Maximizing selectivity. The final inverse problem we consider is an optimal design problem, which aims at designing *in silico* channels with optimal sensitivity properties (or at least improved sensitivity compared to a given initial design but possibly also close to this one, which can be used as a constraining criterion).

As a test case, we use one of the three selectivity measures from [GE02], the so-called permeability ratio, at equal concentrations for all ions in the left and right bath. (For this sake, we use the bath concentrations $\rho_k(\pm L) = 20$ mM for $k = 1, 2$ and $\rho_3(\pm L) = 60$ mM.) More precisely, the selectivity measure is the permeability ratio for Na and Ca, where the permeabilities on the right side of the channel are computed (detailed formulas for the computations of the permeabilities S_a are given in the appendix of [BEE06] and in [GE02]). The unknown to be designed is again related to the structure of the channel; i.e., we set $P = \mu_5^0$ and use the same discretization as in the previous section. Since our design goal is to maximize or at least significantly increase the selectivity, we should minimize the negative permeability ratio. It turns out that formulating the negative permeability ratio $-\frac{S_{Na}(P)}{S_{Ca}(P)}$ as the objective functional for selectivity, one ends up with a very unstable problem (which is also expected from the arguments in section 3.2). Moreover, the computed designs seem not really useful for practical construction due to various oscillations. Therefore, we use an additional regularization term as proposed in (5.9),

$$(6.1) \quad J_\alpha(P) := -\frac{S_{Na}(P)}{S_{Ca}(P)} + \alpha \|P - P^*\|_2 \rightarrow \min_P,$$

where $P = \mu_5^0$ is the confining potential to be optimized and P^* is the favored initial design of the confining potential (the one used in the simulations in [GE02]). Besides its regularizing effect, the second term in the objective functional favors solutions as close as possible to the initial design, which helps to obtain potentials that can be realized in practice.

The objective functional is then minimized with a gradient method and suitable step-size selection to guarantee decrease of the objective, and the gradients are again approximated by finite differences (see above for a discussion of this point).

A special design case (with parameter $\alpha = 200$) is illustrated in the plot in Figure 14 (left), which shows the evolution of the objective functional (black) as well as its first part, the negative permeability (i.e., selectivity) ratio $-\frac{S_{Na}(P)}{S_{Ca}(P)}$, during the iteration until convergence. One observes that an increase in the selectivity measure of more than 100% is achieved by the optimization. The initial value used for the optimization and the final result are plotted in Figure 15. One observes that the two potentials are still very close, and so the structure has not been changed completely.

For comparison (and illustration of instabilities), the classical approach of just minimizing the negative permeability (i.e., selectivity) ratio is also illustrated with the same initial value and parameter settings but with the objective functional $J(P) := -\frac{S_{Na}(P)}{S_{Ca}(P)}$. Again, the right plot in Figure 14 displays the objective functional during the iterations; the optimal solution is plotted in Figure 16. One observes that in this

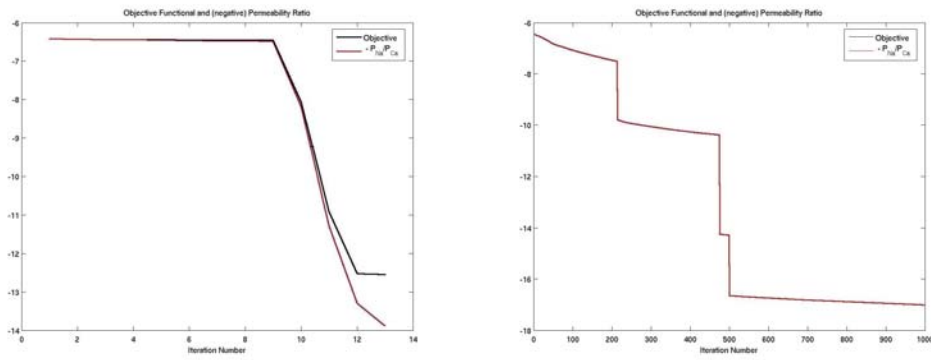


FIG. 14. Objective functional $J_\alpha(P_n)$ (black) and negative permeability ratio (grey; red online) as a function of the iteration number for $\alpha = 200$ (left) and $\alpha = 0$ (right).

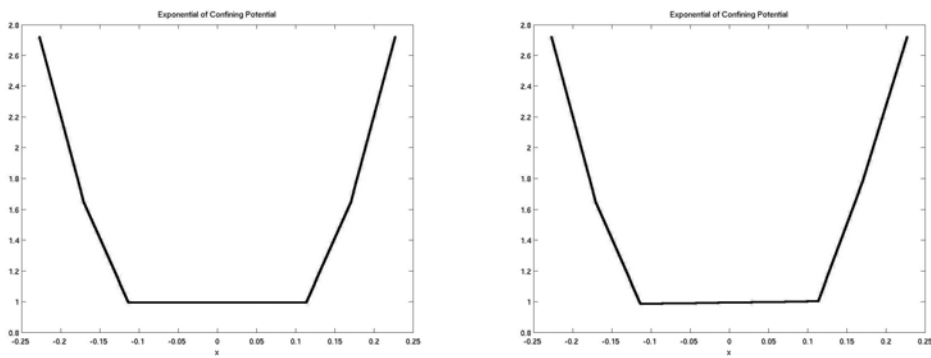


FIG. 15. Initial value (left) and computed optimal confining potential (right) for the functional J_α with $\alpha = 200$.

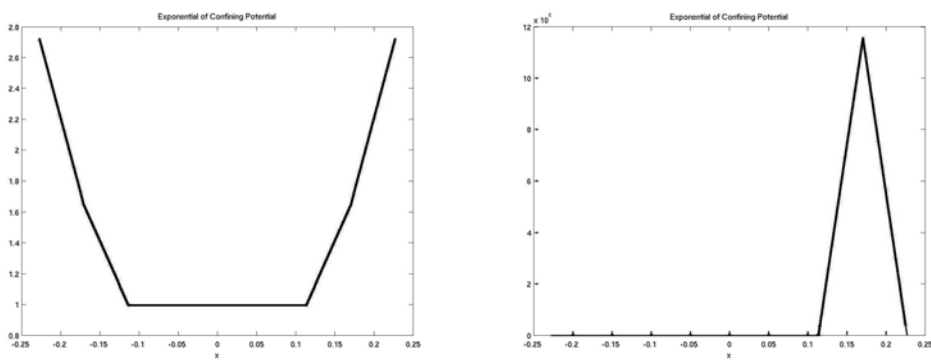


FIG. 16. Initial value (left) and computed optimal confining potential (right) for the functional J .

case, the gradient method needs many more iterations than with penalization but does not yield a dramatic increase of selectivity ratio (around 17 instead of 14 for the penalized case). However, just one look at the optimal confining potential in the

unpenalized case (Figure 16) shows that the (small) increase in the ratio is caused by a blowup in the confining potential (notice the vertical scale of $10^6!$). Obviously, such extremely high forces will not be easy to realize, and the resulting channel will not be useful in practice, which is another point in favor of our regularization approach. The regularization parameter α can control the balance between increasing the selectivity and “practicability,” namely, remaining close enough to the initial design that the new channel can actually be built. If α is very large, then the minimizer of J_α will remain close to the initial guess. For $\alpha \rightarrow 0$, the permeability ratio can be increased further, but also the optimal confining potential will increase more and more (until it reaches the one computed for J in the limit). So, regularization gives (in addition to the advantages discussed) even more flexibility in finding a compromise between different design goals.

We summarize by stating that our examples show that both the identification and the design goals can be achieved in a stable and efficient way by our approach based on regularization, as illustrated by the special case using Tikhonov regularization with an iterative minimization of the Tikhonov functional, and that such results are not possible by standard approaches due the ill-posed nature of the inverse problems considered. It will be interesting to see how regularization methods help in the solution of a range of problems in ion channels and proteins.

REFERENCES

- [Aletal94] B. ALBERTS, D. BRAY, J. LEWIS, M. RAFF, K. ROBERTS, AND J. D. WATSON, *Molecular Biology of the Cell*, Garland, New York, 1994.
- [As99] F. M. ASHCROFT, *Ion Channels and Disease*, Academic Press, New York, 1999.
- [At79] D. ATTWELL, *Problems in the interpretation of membrane current-voltage relations*, in Membrane Transport Processes, Vol. 3, C. F. Stevens and R. W. Tsien, eds., Raven Press, New York, 1979, pp. 21–41.
- [AJ78] D. ATTWELL AND J. J. B. JACK, *The interpretation of membrane current voltage relations: A Nernst-Planck analysis*, Prog. Biophys. Mol. Biol., 34 (1978), pp. 81–107.
- [BeSt98] F. BEZANILLA AND E. STEFANI, *Gating currents*, Methods Enzymol., 293 (1998), pp. 331–352.
- [Beta06] D. BODA, M. VALISKO, B. EISENBERG, W. NONNER, D. HENDERSON, AND D. GILLESPIE, *Effect of protein dielectric coefficient on the ionic selectivity of a calcium channel*, J. Chem. Phys., 125 (2006), 034901.
- [BEE06] M. BURGER, B. EISENBERG, AND H. W. ENGL, *Mathematical Design of Ion Channel Selectivity via Inverse Problems Technology*, U.S. Patent Application, Serial Number 60/791,185.
- [BELM04] M. BURGER, H. W. ENGL, A. LEITAO, AND P. MARKOWICH, *On inverse problems for semiconductor equations*, Milan J. Math., 72 (2004), pp. 273–314.
- [BEM02] M. BURGER, H. W. ENGL, AND P. MARKOWICH, *Inverse doping problems for semiconductor devices*, in Recent Progress in Computational and Applied PDEs, T. F. Chan, Y. Huang, T. Tang, J. A. Xu, and L. A. Ying, eds., Kluwer, Boston, Dordrecht, London, 2002, pp. 39–54.
- [BEMP01] M. BURGER, H. W. ENGL, P. MARKOWICH, AND P. PIETRA, *Identification of doping profiles in semiconductor devices*, Inverse Problems, 17 (2001), pp. 1765–1795.
- [BM02] M. BURGER AND W. MÜHLHUBER, *Numerical approximation of an SQP-type method for parameter identification*, SIAM J. Numer. Anal., 40 (2002), pp. 1775–1797.
- [BP03] M. BURGER AND R. PINNAU, *Fast optimal design of semiconductor devices*, SIAM J. Appl. Math., 64 (2003), pp. 108–126.
- [BW07] M. BURGER AND M. T. WOLFRAM, *Symmetric Discretization of PNP-Systems*, manuscript.
- [CE93] D. P. CHEN AND R. S. EISENBERG, *Charges, currents and potentials in ionic channels of one conformation*, Biophys. J., 64 (1993), pp. 1405–1421.
- [CER90] D. COLTON, R. EWING, AND W. RUNDELL, *Inverse Problems in Partial Differential*

- Equations*, SIAM, Philadelphia, 1990.
- [De85] K. DEIMLING, *Nonlinear Functional Analysis*, Springer, Berlin, 1985.
- [Ei90] R. S. EISENBERG, *Channels as enzymes*, *J. Memb. Biol.*, 115 (1990), pp. 1–12.
- [Ei98] R. S. EISENBERG, *Ionic channels in biological membranes. Electrostatic analysis of a natural nanotube*, *Contemp. Phys.*, 39 (1998), pp. 447–466.
- [En97] H. ENGL, *Integralgleichungen*, Springer, Wien, 1997.
- [EHN96] H. W. ENGL, M. HANKE, AND A. NEUBAUER, *Regularization of Inverse Problems*, Kluwer Academic Publishers, Dordrecht, 1996.
- [EKN89] H. W. ENGL, K. KUNISCH, AND A. NEUBAUER, *Convergence rates for Tikhonov regularization of nonlinear ill-posed problems*, *Inverse Problems*, 5 (1989), pp. 523–540.
- [ER95] H. W. ENGL AND W. RUNDELL, EDs., *Inverse Problems in Diffusion Processes*, SIAM, Philadelphia, 1995.
- [ES00] H. W. ENGL AND O. SCHERZER, *Convergence rate results for iterative methods for solving nonlinear ill-posed problems*, in *Surveys on Solution Methods for Inverse Problems*, D. Colton, H. W. Engl, A. K. Louis, J. McLaughlin, and W. F. Rundell, eds., Springer, Vienna, New York, 2000, pp. 7–34.
- [GE02] D. GILLESPIE AND R. EISENBERG, *Physical descriptions of experimental selectivity measurements in ion channels*, *Eur. Biophys. J.*, 31 (2002), pp. 454–466.
- [GNE02] D. GILLESPIE, W. NONNER, AND R. EISENBERG, *Coupling Poisson-Nernst-Planck and density functional theory to calculate ion flux*, *J. Phys.: Condens. Matter*, 14 (2002), pp. 12129–12145.
- [GNE03] D. GILLESPIE, W. NONNER, AND R. EISENBERG, *Density functional theory of charged, hard-sphere fluids*, *Phys. Rev. E* (3), 68 (2003), 031503.
- [GP00] M. B. GILES AND N. A. PIERCE, *An introduction to the adjoint approach to design*, *Flow, Turbulence and Combustion*, 65 (2000), pp. 393–415.
- [Gr84] C. W. GROETSCH, *The Theory of Tikhonov Regularization for Fredholm Equations of the First Kind*, Pitman, London, 1984.
- [Hetal92] S. H. HEINEMANN, H. TERLAU, W. STUHMER, K. IMOTO, AND S. NUMA, *Calcium channel characteristics conferred on the sodium channel by single mutations*, *Nature*, 356 (1992), pp. 441–443.
- [Hi01] B. HILLE, *Ionic Channels of Excitable Membranes*, Sinauer Associates, Sunderland, MA, 2001.
- [HP02a] M. HINZE AND R. PINNAU, *Optimal control of the drift-diffusion model for semiconductor devices*, in *Optimal Control of Complex Structures*, K. H. Hoffmann, I. Lasiecka, G. Leugering, and J. Sprekels, eds., Birkhäuser, Basel, Berlin, 2002, pp. 95–106.
- [HP02b] M. HINZE AND R. PINNAU, *An optimal control approach to semiconductor design*, *Math. Models Methods Appl. Sci.*, 12 (2002), pp. 89–107.
- [IR02a] W. IM AND S. ROUX, *Ion permeation and selectivity of OmpF porin: A theoretical study based on molecular dynamics, Brownian dynamics, and continuum electrodiffusion theory*, *J. Mol. Biol.*, 322 (2002), pp. 851–869.
- [IR02b] W. IM AND S. ROUX, *Ions and counterions in a biological channel: A molecular dynamics simulation of OmpF porin from Escherichia coli in an explicit membrane with 1 M KCl aqueous salt solution*, *J. Mol. Biol.*, 319 (2002), pp. 1177–1197.
- [IS05] V. ISAKOV, *Inverse Problems for Partial Differential Equations*, 2nd ed., Springer, New York, 2005.
- [JaLu89] C. JACOBONI AND P. LUGLI, *The Monte Carlo Method for Semiconductor Device Simulation*, Springer, New York, 1989.
- [KNS06] B. KALTENBACHER, A. NEUBAUER, AND O. SCHERZER, *Iterative Regularization Methods for Nonlinear Ill-Posed Problems*, manuscript, Johannes Kepler University, Linz, Austria, 2007.
- [KMS83] P. G. KOSTYUK, S. L. MIRONOV, AND Y. M. SHUBA, *Two ion-selective filters in the calcium channel of the somatic membrane of mollusc neurons*, *J. Memb. Biol.*, 76 (1983), pp. 83–93.
- [LHJR00] F. LEHMANN-HORN AND K. JURKAT-ROTT, *Channelopathies*, Elsevier Science, New York, 2000.
- [LMZ06] A. LEITAO, P. A. MARKOWICH, AND J. ZUBELLI, *On the inverse doping profile problems for the voltage-current map*, *Inverse Problems*, 22 (2006), pp. 1071–1088.
- [Maetal03] A. B. MAMONOV, R. D. COALSON, A. NITZAN, AND M. G. KURNIKOVA, *The role of the dielectric barrier in narrow biological channels: A novel composite approach to modeling single-channel currents*, *Biophys. J.*, 84 (2003), pp. 3646–3661.

- [MRS90] P. A. MARKOWICH, C. A. RINGHOFER, AND C. SCHMEISER, *Semiconductor Equations*, Springer, Wien, New York, 1990.
- [Mietal04] H. MIEDEMA, A. METER-ARKEMA, J. WIERENGA, J. TANG, B. EISENBERG, W. NONNER, H. HEKTOR, D. GILLESPIE, AND W. MEIJBERG, *Permeation properties of an engineered bacterial OmpF porin containing the EEEE-locus of Ca²⁺ channels*, *Biophys. J.*, 87 (2004), pp. 3137–3147.
- [Mietal06] H. MIEDEMA, M. VROUENRAETS, J. WIERENGA, R. S. EISENBERG, D. GILLESPIE, W. MEIJBERG, AND W. NONNER, *Ca²⁺ selectivity of a chemically modified OmpF with reduced pore volume*, *Biophys. J.*, 91 (2006), pp. 4392–4400.
- [NHE03] B. NADLER, U. HOLLERBACH, AND R. S. EISENBERG, *Dielectric boundary force and its crucial role in gramicidin*, *Phys. Rev. E Stat. Nonlin. Soft Matter Phys.*, 68 (2003), 021905.
- [Na06] F. NATTERER, *Imaging and Inverse Problems of Partial Differential Equations*, preprint, University of Münster, Münster, Germany, <http://wwwmath1.uni-muenster.de/num/Preprints/2006/artikel.pdf> (2006).
- [NCE00] W. NONNER, L. CATACUZZENO, AND R. EISENBERG, *Binding and selectivity in L-type Ca channels: A mean spherical approximation*, *Biophys. J.*, 79 (2000), pp. 1976–1992.
- [NPGEO4] W. NONNER, A. PEYSER, D. GILLESPIE, AND B. EISENBERG, *Relating microscopic charge movement to macroscopic currents: The Ramo-Shockley theorem applied to ion channels*, *Biophys. J.*, 87 (2004), pp. 3716–3722.
- [OBGXY05] S. OSHER, M. BURGER, D. GOLDFARB, J. XU, AND W. YIN, *An iterative regularization method for total variation-based image restoration*, *Multiscale Model. Simul.*, 4 (2005), pp. 460–489.
- [Ru90] I. RUBINSTEIN, *Electro-diffusion of Ions*, SIAM, Philadelphia, 1990.
- [SMC03] W. A. SATHER AND E. W. MCCLESKEY, *Permeation and selectivity in calcium channels*, *Annu. Rev. Physiol.*, 65 (2003), pp. 133–159.
- [Sch98] O. SCHERZER, *An iterative multi-level algorithm for solving nonlinear ill-posed problems*, *Numer. Math.*, 80 (1998), pp. 579–600.
- [SNE01] Z. SCHUSS, B. NADLER, AND R. S. EISENBERG, *Derivation of PNP equations in bath and channel from a molecular model*, *Phys. Rev. E* (3), 64 (2001), 036111.
- [SV89] T. I. SEIDMAN AND C. R. VOGEL, *Well-posedness and convergence of some regularization methods for nonlinear ill-posed problems*, *Inverse Problems*, 5 (1989), pp. 227–238.
- [Se84] S. SELBERHERR, *Analysis and Simulation of Semiconductor Devices*, Springer, New York, 1984.
- [Sietal06] Z. S. SIWY, M. R. POWELL, A. PETROV, E. KALMAN, C. TRAUTMANN, AND R. S. EISENBERG, *Calcium-induced voltage gating in single conical nanopores*, *Nano Lett.*, 6 (2006), pp. 1729–1734.
- [Sh96] R. E. SHOWALTER, *Nonlinear Partial Differential Equations and Monotone Operators in Banach Space*, AMS, Providence, RI, 1996.
- [TBSS01] D. P. TIELEMAN, P. C. BIGGIN, G. R. SMITH, AND M. S. SANSOM, *Simulation approaches to ion channel structure-function relationships*, *Q. Rev. Biophys.*, 34 (2001), pp. 473–561.
- [VR50] W. R. VAN ROOSBROECK, *Theory of flow of electrons and holes in germanium and other semiconductors*, *Bell System Tech. J.*, 29 (1950), pp. 560–607.
- [Waetal05] Y. WANG, L. XU, D. PASEK, D. GILLESPIE, AND G. MEISSNER, *Probing the role of negatively charged amino acid residues in ion permeation of skeletal muscle ryanodine receptor*, *Biophys. J.*, 89 (2005), pp. 256–265.
- [We68] H. WEYL, *Gesammelte Abhandlungen*, Springer, Berlin, 1968.
- [Wo06] M. T. WOLFRAM, *Semiconductor Inverse Dopant Profiling from Transient Measurements*, SFB Technical Report 2006-4 (SFB F013), Johannes Kepler University, Linz, Austria, 2006, submitted.
- [WB06] M. T. WOLFRAM AND M. BURGER, *Inverse dopant profiling for highly doped semiconductor devices*, in *Proceedings of the 5th MATHMOD Conference*, F. Breitenecker and I. Troch, eds., Vienna, Austria, 2006.
- [XWGM06] L. XU, Y. WANG, D. GILLESPIE, AND G. MEISSNER, *Two rings of negative charges in the cytosolic vestibule of type-1 ryanodine receptor modulate ion fluxes*, *Biophys. J.*, 90 (2006), pp. 443–453.